Research Article | Vol. 24, No. 15 | 25 Jul 2016 | OPTICS EXPRESS 17138

Optics EXPRESS

Controlling the nonlinear optical properties of plasmonic nanoparticles with the phase of their linear response

JÉRÉMY BUTET,* T. V. RAZIMAN, KUANG-YU YANG, GABRIEL D. BERNASCONI, AND OLIVIER J. F. MARTIN

Nanophotonics and Metrology Laboratory (NAM), Swiss Federal Institute of Technology Lausanne (EPFL),1015, Lausanne, Switzerland
**jeremy.butet@epfl.ch*

Abstract: We numerically investigate the second harmonic generation from different plasmonic systems and evidence the key role played in their nonlinear response by the phase at the fundamental wavelength. In the case of a single plasmonic nanorod, the interference between the second harmonic dipolar and quadrupolar emission modes depends on their relative phase, which is deeply related to the excitation wavelength. The knowledge obtained in this simple case is then used to describe and understand the nonlinear response from a more complex structure, namely a gold nanodolmen. The complex phase evolution associated with a Fano resonance arising at the fundamental wavelength enables dramatically modifying the second harmonic emission patterns from plasmonic metamolecules within minute wavelength shifts. These results emphasize the importance of the phase in the nonlinear optical processes arising in plasmonic nanostructures, in addition to the increase in conversion yield associated with the excitation of localized surface plasmon resonances.

OCIS codes: (160.3900) Metals; (190.0190) Nonlinear optics; (190.2620) Harmonic generation and mixing; (160.4236) Nanomaterials.

References and links

1. W. L. Barnes, A. Dereux, and T. W. Ebbesen, "Surface plasmon subwavelength optics," Nature **424**(6950), 824–830 (2003).
2. M. I. Stockman, "Nanoplasmonics: Past, present, and glimpse into future," Opt. Express **19**(22), 22029–22106 (2011).
3. S. A. Maier, *Plasmonics: Fundamentals and Applications* (Springer, 2007).
4. J. A. Schuller, E. S. Barnard, W. Cai, Y. C. Jun, J. S. White, and M. L. Brongersma, "Plasmonics for extreme light concentration and manipulation," Nat. Mater. **9**(3), 193–204 (2010).
5. O. J. F. Martin, C. Girard, and A. Dereux, "Generalized field propagator for electromagnetic scattering and light confinement," Phys. Rev. Lett. **74**(4), 526–529 (1995).
6. E. Prodan, C. Radloff, N. J. Halas, and P. Nordlander, "A hybridization model for the plasmon response of complex nanostructures," Science **302**(5644), 419–422 (2003).
7. N. J. Halas, S. Lal, W. S. Chang, S. Link, and P. Nordlander, "Plasmons in strongly coupled metallic nanostructures," Chem. Rev. **111**(6), 3913–3961 (2011).
8. P. Nordlander, C. Oubre, E. Prodan, K. Li, and M. I. Stockman, "Plasmon hybridization in nanoparticle dimers," Nano Lett. **4**(5), 899–903 (2004).
9. P. K. Jain, W. Huang, and M. A. El-Sayed, "On the universal scaling behavior of the distance decay of plasmon coupling in metal nanoparticle pairs: a plasmon ruler equation," Nano Lett. **7**(7), 2080–2088 (2007).
10. B. Luk'yanchuk, N. I. Zheludev, S. A. Maier, N. J. Halas, P. Nordlander, H. Giessen, and C. T. Chong, "The Fano resonance in plasmonic nanostructures and metamaterials," Nat. Mater. **9**(9), 707–715 (2010).
11. A. E. Miroshnichenko, S. Flach, and Y. S. Kivshar, "Fano resonances in nanoscale structures," Rev. Mod. Phys. **82**(3), 2257–2298 (2010).
12. F. Hao, P. Nordlander, Y. Sonnefraud, P. Van Dorpe, and S. A. Maier, "Tunability of subradiant dipolar and fano-type plasmon resonances in metallic ring/disk cavities: Implications for nanoscale optical sensing," ACS Nano **3**(3), 643–652 (2009).
13. Y. H. Fu, J. B. Zhang, Y. F. Yu, and B. Luk'yanchuk, "Generating and manipulating higher order Fano resonances in dual-disk ring plasmonic nanostructures," ACS Nano **6**(6), 5130–5137 (2012).
14. A. E. Cetin and H. Altug, "Fano resonant ring/disk plasmonic nanocavities on conducting substrates for advanced biosensing," ACS Nano **6**(11), 9989–9995 (2012).

#264319 http://dx.doi.org/10.1364/OE.24.017138
Journal © 2016 Received 29 Apr 2016; revised 8 Jul 2016; accepted 8 Jul 2016; published 20 Jul 2016

Optics EXPRESS

15. C. Wu, A. B. Khanikaev, R. Adato, N. Arju, A. A. Yanik, H. Altug, and G. Shvets, "Fano-resonant asymmetric metamaterials for ultrasensitive spectroscopy and identification of molecular monolayers," Nat. Mater. **11**(1), 69–75 (2011).
16. N. Verellen, Y. Sonnefraud, H. Sobhani, F. Hao, V. V. Moshchalkov, P. Van Dorpe, P. Nordlander, and S. A. Maier, "Fano resonances in individual coherent plasmonic nanocavities," Nano Lett. **9**(4), 1663–1667 (2009).
17. N. Liu, T. Weiss, M. Mesch, L. Langguth, U. Eigenthaler, M. Hirscher, C. Sönnichsen, and H. Giessen, "Planar metamaterial analogue of electromagnetically induced transparency for plasmonic sensing," Nano Lett. **10**(4), 1103–1107 (2010).
18. J. A. Fan, C. Wu, K. Bao, J. Bao, R. Bardhan, N. J. Halas, V. N. Manoharan, P. Nordlander, G. Shvets, and F. Capasso, "Self-assembled plasmonic nanoparticle clusters," Science **328**(5982), 1135–1138 (2010).
19. J. B. Lassiter, H. Sobhani, J. A. Fan, J. Kundu, F. Capasso, P. Nordlander, and N. J. Halas, "Fano resonances in plasmonic nanoclusters: geometrical and chemical tunability," Nano Lett. **10**(8), 3184–3189 (2010).
20. M. Hentschel, M. Saliba, R. Vogelgesang, H. Giessen, A. P. Alivisatos, and N. Liu, "Transition from isolated to collective modes in plasmonic oligomers," Nano Lett. **10**(7), 2721–2726 (2010).
21. M. Hentschel, D. Dregely, R. Vogelgesang, H. Giessen, and N. Liu, "Plasmonic oligomers: the role of individual particles in collective behavior," ACS Nano **5**(3), 2042–2050 (2011).
22. B. Gallinet and O. J. F. Martin, "Ab-initio theory of Fano resonances in plasmonic nanostructures and metamaterials," Phys. Rev. B **83**(23), 235427 (2011).
23. B. Gallinet and O. J. F. Martin, "Influence of electromagnetic interactions on the line shape of plasmonic Fano resonances," ACS Nano **5**(11), 8999–9008 (2011).
24. V. Giannini, Y. Francescato, H. Amrania, C. C. Phillips, and S. A. Maier, "Fano resonances in nanoscale plasmonic systems: a parameter-free modeling approach," Nano Lett. **11**(7), 2835–2840 (2011).
25. M. Rahmani, D. Y. Lei, V. Giannini, B. Lukiyanchuk, M. Ranjbar, T. Y. F. Liew, M. Hong, and S. A. Maier, "Subgroup decomposition of plasmonic resonances in hybrid oligomers: Modeling the resonance lineshape," Nano Lett. **12**(4), 2101–2106 (2012).
26. A. Lovera, B. Gallinet, P. Nordlander, and O. J. F. Martin, "Mechanisms of Fano resonances in coupled plasmonic systems," ACS Nano **7**(5), 4527–4536 (2013).
27. M. Kauranen and A. V. Zayats, "Nonlinear plasmonics," Nat. Photonics **6**(11), 737–748 (2012).
28. J. Butet, P.-F. Brevet, and O. J. F. Martin, "Optical second harmonic generation in plasmonic nanostructures: From fundamental principles to advanced applications," ACS Nano **9**(11), 10545–10562 (2015).
29. A. Bouhelier, M. Beversluis, A. Hartschuh, and L. Novotny, "Near-field second-harmonic generation induced by local field enhancement," Phys. Rev. Lett. **90**(1), 013903 (2003).
30. R. Jin, J. E. Jureller, H. Y. Kim, and N. F. Scherer, "Correlating second harmonic optical responses of single Ag nanoparticles with morphology," J. Am. Chem. Soc. **127**(36), 12482–12483 (2005).
31. V. K. Valev, N. Smisdom, A. V. Silhanek, B. De Clercq, W. Gillijns, M. Ameloot, V. V. Moshchalkov, and T. Verbiest, "Plasmonic ratchet wheels: switching circular dichroism by arranging chiral nanostructures," Nano Lett. **9**(11), 3945–3948 (2009).
32. J. Butet, J. Duboisset, G. Bachelier, I. Russier-Antoine, E. Benichou, C. Jonin, and P.-F. Brevet, "Optical second harmonic generation of single metallic nanoparticles embedded in a homogeneous medium," Nano Lett. **10**(5), 1717–1721 (2010).
33. J. Butet, G. Bachelier, I. Russier-Antoine, C. Jonin, E. Benichou, and P.-F. Brevet, "Interference between selected dipoles and octupoles in the optical second-harmonic generation from spherical gold nanoparticles," Phys. Rev. Lett. **105**(7), 077401 (2010).
34. Y. Zhang, N. K. Grady, C. Ayala-Orozco, and N. J. Halas, "Three-dimensional nanostructures as highly efficient generators of second harmonic light," Nano Lett. **11**(12), 5519–5523 (2011).
35. H. Husu, R. Siikanen, J. Mäkitalo, J. Lehtolahti, J. Laukkanen, M. Kuittinen, and M. Kauranen, "Metamaterials with tailored nonlinear optical response," Nano Lett. **12**(2), 673–677 (2012).
36. R. Czaplicki, H. Husu, R. Siikanen, J. Mäkitalo, M. Kauranen, J. Laukkanen, J. Lehtolahti, and M. Kuittinen, "Enhancement of second-harmonic generation from metal nanoparticles by passive elements," Phys. Rev. Lett. **110**(9), 093902 (2013).
37. S. Kruk, M. Weismann, A. Y. Bykov, E. A. Mamonov, I. A. Kolmychek, T. Murzina, N. C. Panoiu, D. N. Neshev, and Y. S. Kivshar, "Enhanced magnetic second-harmonic generation from resonant metasurfaces," ACS Photonics **2**(8), 1007–1012 (2015).
38. D. de Ceglia, M. A. Vincenti, C. De Angelis, A. Locatelli, J. W. Haus, and M. Scalora, "Role of antenna modes and field enhancement in second harmonic generation from dipole nanoantennas," Opt. Express **23**(2), 1715–1729 (2015).
39. B. Metzger, L. Gui, J. Fuchs, D. Floess, M. Hentschel, and H. Giessen, "Strong enhancement of second harmonic emission by plasmonic resonances at the second harmonic wavelength," Nano Lett. **15**(6), 3917–3922 (2015).
40. J. Butet, I. Russier-Antoine, C. Jonin, N. Lascoux, E. Benichou, and P.-F. Brevet, "Sensing with multipolar second harmonic generation from spherical metallic nanoparticles," Nano Lett. **12**(3), 1697–1701 (2012).
41. G. Bautista, M. J. Huttunen, J. Mäkitalo, J. M. Kontio, J. Simonen, and M. Kauranen, "Second-harmonic generation imaging of metal nano-objects with cylindrical vector beams," Nano Lett. **12**(6), 3207–3212 (2012).
42. J. Butet, K. Thyagarajan, and O. J. F. Martin, "Ultrasensitive optical shape characterization of gold nanoantennas using second harmonic generation," Nano Lett. **13**(4), 1787–1792 (2013).

Optics EXPRESS

43. J. Butet and O. J. F. Martin, "Nonlinear plasmonic nanorulers," ACS Nano **8**(5), 4931–4939 (2014).
44. V. K. Valev, A. V. Silhanek, W. Gillijns, Y. Jeyaram, H. Paddubrouskaya, A. Volodin, C. G. Biris, N. C. Panoiu, B. De Clercq, M. Ameloot, O. A. Aktsipetrov, V. V. Moshchalkov, and T. Verbiest, "Plasmons reveal the direction of magnetization in nickel nanostructures," ACS Nano **5**(1), 91–96 (2011).
45. M. Bertolotti, A. Belardini, A. Benedetti, and C. Sibilia, "Second harmonic circular dichroism by self-assembled metasurfaces [Invited]," J. Opt. Am. Soc. B **32**(7), 1287–1293 (2015).
46. J. W. Jarrett, T. Zhao, J. S. Johnson, and K. L. Knappenberger, Jr., "Investigating plasmonic structure-dependent light amplification and electronic dynamics using advances in nonlinear optical microscopy," J. Phys. Chem. C **119**(28), 15779–15800 (2015).
47. A. Anderson, K. S. Deryckx, X. G. Xu, G. Steinmeyer, and M. B. Raschke, "Few-femtosecond plasmon dephasing of a single metallic nanostructure from optical response function reconstruction by interferometric frequency resolved optical gating," Nano Lett. **10**(7), 2519–2524 (2010).
48. S. Berweger, J. M. Atkin, X. G. Xu, R. L. Olmon, and M. B. Raschke, "Femtosecond nanofocusing with full optical waveform control," Nano Lett. **11**(10), 4309–4313 (2011).
49. M.-K. Kim, H. Sim, S. J. Yoon, S.-H. Gong, C. W. Ahn, Y.-H. Cho, and Y.-H. Lee, "Squeezing photons into a point-like space," Nano Lett. **15**(6), 4102–4107 (2015).
50. H. Harutyunyan, G. Volpe, R. Quidant, and L. Novotny, "Enhancing the nonlinear optical response using multifrequency gold-nanowire antennas," Phys. Rev. Lett. **108**(21), 217403 (2012).
51. K. Thyagarajan, S. Rivier, A. Lovera, and O. J. F. Martin, "Enhanced second-harmonic generation from double resonant plasmonic antennae," Opt. Express **20**(12), 12860–12865 (2012).
52. H. Aouani, M. Navarro-Cia, M. Rahmani, T. P. H. Sidiropoulos, M. Hong, R. F. Oulton, and S. A. Maier, "Multiresonant broadband optical antennas as efficient tunable nanosources of second harmonic light," Nano Lett. **12**(9), 4997–5002 (2012).
53. K. Thyagarajan, J. Butet, and O. J. F. Martin, "Augmenting second harmonic generation using Fano resonances in plasmonic systems," Nano Lett. **13**(4), 1847–1851 (2013).
54. A. M. Kern and O. J. F. Martin, "Surface integral formulation for 3D simulations of plasmonic and high permittivity nanostructures," J. Opt. Soc. Am. A **26**(4), 732–740 (2009).
55. P. B. Johnson and R. W. Christy, "Optical constants of the noble metals," Phys. Rev. B **6**(12), 4370–4379 (1972).
56. P. G. Etchegoin, E. C. Le Ru, and M. Meyer, "An analytic model for the optical properties of gold," J. Chem. Phys. **125**(16), 164705 (2006).
57. T. V. Raziman, O. J. F. Martin, "Does the real part contain all the physical information?" In preparation.
58. J. Mäkitalo, S. Suuriniemi, and M. Kauranen, "Boundary element method for surface nonlinear optics of nanoparticles," Opt. Express **19**(23), 23386–23399 (2011).
59. G. Bachelier, J. Butet, I. Russier-Antoine, C. Jonin, E. Benichou, and P.-F. Brevet, "Origin of optical second-harmonic generation in spherical gold nanoparticles: Local surface and nonlocal bulk contribution," Phys. Rev. B **82**(23), 235403 (2010).
60. F. X. Wang, F. J. Rodriguez, W. M. Albers, R. Ahorinta, J. E. Sipe, and M. Kauranen, "Surface and bulk contributions to the second-order nonlinear optical response of a gold film," Phys. Rev. B **80**(23), 233402 (2009).
61. T. F. Heinz, "Second-order nonlinear optical effects at surfaces and interfaces," in *Nonlinear Surface Electromagnetic Phenomena*, H.-E. Ponath and G. I. Stegeman ed. (Elsevier, 1991).
62. T. V. Raziman and O. J. F. Martin, "Polarisation charges and scattering behaviour of realistically rounded plasmonic nanostructures," Opt. Express **21**(18), 21500–21507 (2013).
63. C. F. Bohren and D. R. Huffman, *Absorption and Scattering of Light by Small Particles* (Wiley, 1983).
64. K. O'Brien, H. Suchowski, J. Rho, A. Salandrino, B. Kante, X. Yin, and X. Zhang, "Predicting nonlinear properties of metamaterials from the linear response," Nat. Mater. **14**(4), 379–383 (2015).
65. C. Hubert, L. Billot, P.-M. Adam, R. Bachelot, P. Royer, J. Grand, D. Gindre, K. D. Dorhenoo, and A. Fort, "Role of surface plasmon in second harmonic generation from gold nanorods," Appl. Phys. Lett. **90**(18), 181105 (2007).
66. A. Singh, A. Lehoux, H. Remita, J. Zyss, and I. Ledoux-Rak, "Second harmonic response of gold nanorods: A strong enhancement with the aspect ratio," J. Phys. Chem. Lett. **4**(22), 3958–3961 (2013).
67. Y. El Harfouch, E. Benichou, F. Bertorelle, I. Russier-Antoine, C. Jonin, N. Lascoux, and P.-F. Brevet, "Hyper-Rayleigh scattering from gold nanorods," J. Phys. Chem. C **118**(1), 609–616 (2014).
68. S.-B. Hasan, C. Etrich, R. Filter, C. Rockstuhl, and F. Lederer, "Enhancing the nonlinear response of plasmonic nanowire antennas by engineering their terminations," Phys. Rev. B **88**(20), 205125 (2013).
69. J. I. Dadap, J. Shan, K. B. Eisenthal, and T. F. Heinz, "Second-harmonic Rayleigh scattering from a sphere of centrosymmetric material," Phys. Rev. Lett. **83**(20), 4045–4048 (1999).
70. J. I. Dadap, J. Shan, and T. F. Heinz, "Theory of optical second-harmonic generation from a sphere of centrosymmetric material: Small-particle limit," J. Opt. Soc. Am. B **21**(7), 1328 (2004).
71. G. D. Bernasconi, J. Butet, and O. J. F. Martin, "Mode analysis of second harmonic generation in plasmonic nanostructures," J. Opt. Soc. Am. B **33**(4), 768–779 (2016).
72. C. Ciracì, E. Poutrina, M. Scalora, and D. R. Smith, "Origin of second-harmonic generation enhancement in optical split-ring resonators," Phys. Rev. B **85**(20), 201403 (2012).

Optics EXPRESS

73. M. W. Klein, C. Enkrich, M. Wegener, and S. Linden, "Second-harmonic generation from magnetic metamaterials," Science **313**(5786), 502–504 (2006).
74. K.-Y. Yang, J. Butet, and O. J. F. Martin, "Mechanisms of second harmonic generation enhancement in double resonant plasmonic nanostructures," In preparation.
75. A. E. Minovich, A. E. Miroshnichenko, A. Y. Bykov, T. V. Murzina, D. N. Neshev, and Y. S. Kivshar, "Functional and nonlinear optical metasurfaces," Laser Photonics Rev. **9**(2), 195–213 (2015).
76. N. Segal, S. Keren-Zur, N. Hendler, and T. Ellenbogen, "Controlling light with metamaterials-based nonlinear photonic crystals," Nat. Photonics **9**(3), 180–184 (2015).
77. G. Li, S. Chen, N. Pholchai, B. Reineke, P. W. H. Wong, E. Y. B. Pun, K. W. Cheah, T. Zentgraf, and S. Zhang, "Continuous control of the nonlinearity phase for harmonic generations," Nat. Mater. **14**(6), 607–612 (2015).
78. N. Accanto, L. Piatkowski, I. M. Hancu, J. Renger, and N. F. van Hulst, "Resonant plasmonic nanoparticles for multicolor second harmonic imaging," Appl. Phys. Lett. **108**(8), 083115 (2016).
79. T. Shegai, S. Chen, V. D. Miljković, G. Zengin, P. Johansson, and M. Käll, "A bimetallic nanoantenna for directional colour routing," Nat. Commun. **2**, 481 (2011).
80. K. Saito and T. Tatsuma, "Asymmetric three-way plasmonic color routers," Adv. Opt. Mater. **3**(7), 883–887 (2015).

1. Introduction

Plasmonic nanostructures play a key role in nanophotonics thanks to their unique optical properties [1, 2]. Indeed, an exceptional physical phenomenon can be observed in metallic nanoparticles, which corresponds to the collective oscillation of the conduction electrons *i.e.* localized surface plasmon resonances [3]. These resonances result in unique optical properties, especially the localization of light in a nanoscale volume, making them instrumental for the development of applications in nanophotonics [4, 5]. The coupling and hybridization between plasmon modes is a widely used technique for designing their intrinsic properties, *e.g.* the resonant wavelength [6, 7]. In this framework, Fano resonances have been widely investigated, since they offer more possibilities for tailoring the spectral response of plasmonic systems [8, 9]. For example, Fano resonances have been observed in various coupled metallic nanostructures, composed of either nanodiscs or nanorods [10–21]. Beside these experimental observations, specific theoretical models have been proposed, deriving the asymmetric lineshape of Fano resonances from the coupling between optically dark and bright modes [22–24]. Due to the coupling between plasmonic modes with different radiative properties, Fano resonances allow a subtle control of the near-field distribution close to plasmonic nanostructures [8, 9]. One the other hand, the coupling between bright modes can also produce Fano resonances [25, 26].

In parallel to this investigation of the linear optical properties of plasmonic nanostructures, more and more of the published studies discuss their nonlinear optical properties [27]. Among all the different nonlinear optical processes, second harmonic generation (SHG), has been extensively studied, due to its interesting symmetry properties [28–39]. Both centrosymmetric and non-centrosymmetric metallic nanostructures have been investigated and the influence of the nanoparticle shape and retardation effects have been discussed in details [28–39]. Several studies have been performed on single metallic nanostructures, demonstrating that the conversion yield is high enough for the development of practical applications ranging from shape characterization [40–43] to nonlinear imaging [44–46] and the determination of the surface plasmon resonance properties [47–49]. In regards to the development of practical applications, it is also important to increase as much as possible the nonlinear optical conversion at the nanoscale. To reach this goal, multiresonant plasmonic nanostructures, optimizing both the interaction with the pump beam and the radiation of the nonlinear signal, were proposed [50–53]. However, so far only the influence of the *intensity* on the nonlinear conversion in plasmonic structures has been discussed, while the role played by the *phase* in their nonlinear response has been sparsely investigated in the literature [28]. In this article, we address this issue and study the influence of the plasmonic phase on the SHG from a single gold nanorod and a gold nanodolmen composed of three nanorods that support a Fano resonance.

Optics EXPRESS

2. Numerical method

The linear optical responses are calculated using a surface integral equation formulation (SIE) [54]. A plane wave polarized along the *x*-axis and propagating along the *z*-axis is considered throughout this work. All the nanostructures are assumed in vacuum and the dielectric constant for gold are given by the Drude model at the fundamental wavelength and taken from experimental data at the second harmonic (SH) wavelength [55]. In the Drude model, the permittivity of gold is given by:

$$\varepsilon_{Drude}(\omega) = \varepsilon_{\infty} - \frac{\omega_p^2}{\omega(\omega + i\gamma)}, \quad (1)$$

where the Drude parameters are chosen to reproduce the experimental data of Johnson and Christy (ε_{∞} = 9.5, ω_p = 8.95 eV, and γ = 0.0691 eV) [56]. This choice is motivated by the necessity to include the contribution of the interband transitions to the dielectric constant at the SH wavelength and to ease comparison with our previous discussion on the charge distribution in plasmonic nanoparticles [57]. In the SIE for surface SHG computations, the expansion of the linear electric and magnetic surface currents on Rao-Wilton-Glisson (RWG) basis functions is used for the evaluation of the fundamental electric fields just below the gold surfaces, as required for the calculation of the surface SH polarization [54, 58]. Only the component $\chi_{\perp,\perp\perp}$ of the surface tensor (where $\perp$ denotes the component normal to the surface) is considered here since recent experimental results indicate that this term dominates the surface response of gold nanoparticles [59]. It is worth to note that other contributions to the SH signal are theoretically allowed but these other terms contribute only weakly to the total SH wave [59, 60]. Furthermore, the present work is focused on the influence of the phase at the fundamental wavelength on the SH emission patterns and the mechanisms discussed in this article are expected to be valid for the other nonlinear sources. In order to satisfy the boundary conditions at the nanostructure surfaces for the SH fields, a Poggio-Miller-Chang-Harrington-Wu-Tsai formulation, including the nonlinear polarization, is derived [53, 55, 61]. The SH surface currents are then expanded on the same RWG basis functions and the expansion coefficients are found by the method of moments including Galerkin's testing [54, 58]. Both the SH near-field and far-field distributions can be directly computed from the SH surface currents using a two-term subtraction method for the evaluation of the Green's function [54, 58].

3. Results and discussion

3.1 Gold nanorod

The first nanostructure considered in this work is a 120 nm long gold nanorod with a 40 nm x 40 nm square cross section. All the edges and the corners have been rounded with a radius *r* = 5 nm to match fabricated structures better [62]. Both the amplitude and the phase of the longitudinal dipolar moment of the gold nanorod induced by the incoming planewave are shown in Fig. 1(a) as functions of the incident wavelength. The phase of the dipolar moment is defined relatively to the phase of the incident planewave. The amplitude of the dipolar moment is maximal for an incident wavelength close to λ = 652 nm corresponding to the excitation of the longitudinal localized surface plasmon resonance of the nanorod. In addition to the amplitude of the response, the surface plasmon resonance also modifies its phase, as well known in physical resonant systems [63]. For an incident wavelength longer than the resonant wavelength, the plasmonic response is in-phase with the excitation. However, for an incident wavelength shorter than the resonant wavelength, the plasmonic response is out-of-phase with the excitation. To illustrate this point, the normalized real part of polarization charge distribution on the nanorod surface is shown for incident wavelengths longer and

Optics EXPRESS

shorter than the resonant wavelength of the longitudinal dipolar plasmon mode, see Fig. 1(b) where a clear reversal in the charge distribution is visible. The influence of the phase on the linear response of plasmonic systems is often not considered, in particular, because optical detectors are sensitive only to the light intensity, not to its phase. However, in the following, we demonstrate that the linear phase plays a dramatic role in the nonlinear optical conversion and can greatly modify the prediction based only on the amplitude of the fundamental electric field [64].

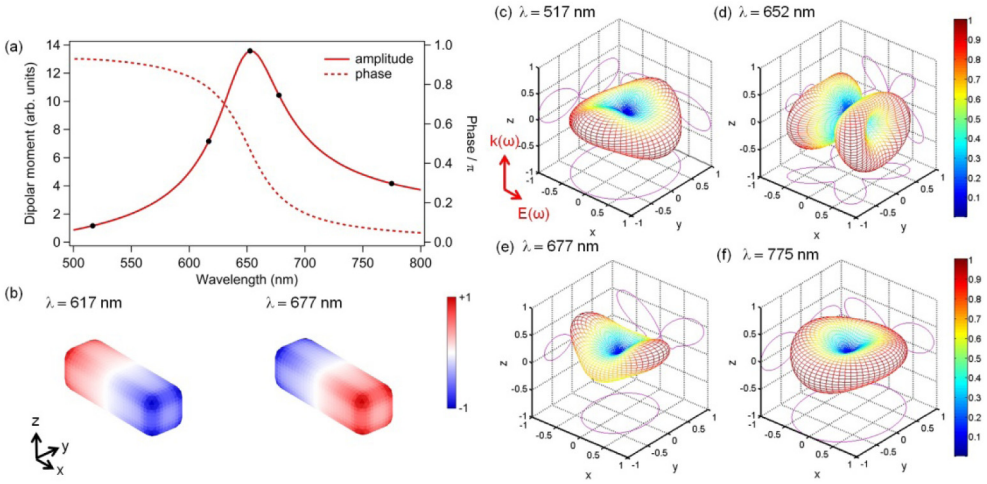

Fig. 1. Linear response of a 120 nm x 40 nm x 40 nm gold nanorod. (a) Amplitude and phase of the linear dipolar moment as functions of the incident wavelength. The incident planewave is polarized along the long nanorod axis. The black dots show the wavelength at which the SHG has been studied. (b) Normalized charge distributions for an excitation wavelength shorter and longer than the dipolar resonant wavelength. Second harmonic emission patterns for the same gold nanorod and for an incident wavelength (c) λ = 517 nm, (d) λ = 652 nm, (e) λ = 677 nm, and (f) λ = 775 nm.

To investigate the role of the phase in the nonlinear generation of light in plasmonic nanoparticles, the SHG from the gold nanorod discussed previously has been computed using the SIE method described in the numerical method section. Note that the influence of the nanorod aspect ratio and shape on the SH intensity has been investigated previously [65–68]. The 3D SH emission patterns have been evaluated for incident wavelengths ranging between 517 nm and 775 nm as shown in Figs. 1(c)–1(f), where each pattern is normalized to its maximum. Note that a maximum of the total SHG (integrated over a 10 μm sphere) is observed close to the maximum of the linear dipolar moment. The investigated spectral range covers the π-phase shift through the longitudinal localized surface plasmon resonance. As expected for a centrosymmetric nanoparticle, the SH intensity vanishes in the forward and backward directions for all the evaluated emission patterns [69, 70]. Note that, despite the fact that the nanoparticle geometry is kept constant, the SH emissio n pattern evolves dramatically with the incident wavelength; underlining that the nanoparticle shape is not the only important parameter in the nonlinear response of a plasmonic system. In order to determine what parameters influence the SH emission pattern, the SH nonlinear polarization has been evaluated on the surface of the gold nanorod, see Fig. 2. Quite surprisingly, except for the shortest incident wavelength (λ = 517 nm), the normalized surface nonlinear polarization distribution is the same for all the incident wavelengths, with the nonlinear sources very strong close to the nanorod corners. This result clearly indicates that the evolution of the SH emission pattern is not induced by a change in the spatial distribution of the SH sources over the nanoparticle surface, as observed recently in Fano resonant metamolecules [43]. At this point, the only parameter that could explain the evolution of the nonlinear response is the

Optics EXPRESS

phase of the nonlinear surface polarization, which is deeply related to the phase of the localized surface plasmon resonance as shown in the following.

Before discussing the role of the phase in detail, it is useful to recall important properties of the SHG in centrosymmetric nanoparticles [69, 70]. Indeed, SHG is forbidden in a centrosymmetric nanoparticle (composed of a centrosymmetric material and with a centrosymmetric shape, such as the gold nanorod discussed here) in the electric dipole approximation. As a first consequence, higher order modes *i.e.* quadrupolar modes must be involved in the description of SHG. The most efficient mechanism for a dipolar SH emission is the $E_1 + E_2 \rightarrow E_1$ mechanism [69, 70]. We use here the standard notation where the two terms on the left of the arrow refer to the nature of the two exciting fundamental modes whereas the right term describes the SH emission mode. Explicitly, this mechanism corresponds to a dipolar emission E_1 arising from the combination of an electric dipolar E_1 and an electric quadrupolar mode E_2, see Figs. 3(a) and 3(b). To understand the schematic charge distributions in this figure, recall that the charge distribution corresponding to the SH mode is obtained by multiplying the charges for both fundamental modes, as it is the case for the fundamental electric field in the computation of the nonlinear polarization. For example, in Fig. 3(a), the negative charge in the top left corner of E_1 is multiplied with the negative charge in the top left corner of E_2, producing the positive charge in the corresponding location for the SH mode E_1. The $E_1 + E_1 \rightarrow E_1$ mechanism, *i.e.* the lowest order mode of the SH emission, is forbidden here because we consider a centrosymmetric system and this mechanism would not preserve the overall parity of the SHG process. To exist, the SH dipolar emission requires a retardation effect at the fundamental frequency, which can be obtained by the introduction of the quadrupolar mode. On the other hand, the quadrupolar mode for the SH emission can be excited without retardation effects at the fundamental frequency, neglecting the spatial variation of the incident planewave, since this mode arises from the $E_1 + E_1 \rightarrow E_2$ mechanism [71].

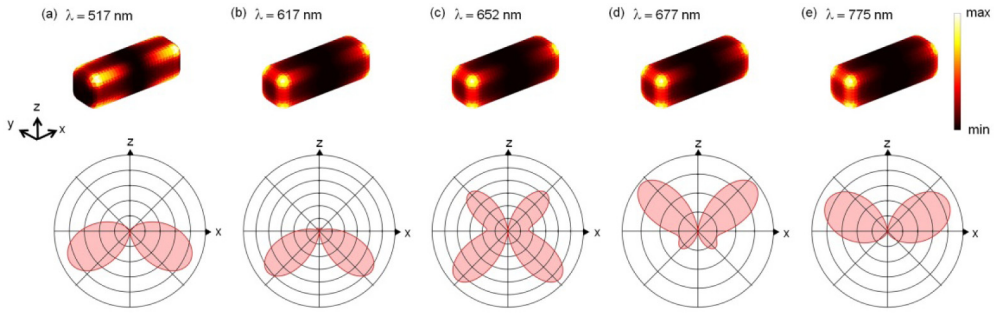

Fig. 2. Nonlinear polarization distribution on the surface of a gold nanorod and the corresponding SH emission patterns in the (O, *x*, *z*) plane for different incident wavelengths: (a) λ = 517 nm, (b) λ = 617 nm, (c) λ = 652 nm, (d) λ = 677 nm, and (e) λ = 775 nm.

With these mode combinations in mind, it is now easier to examine why and how the linear phase modifies the SH emission pattern. To make this process even simpler, the 3D SH emission patterns have been reduced to 2D polar plots, corresponding to the SH emission in the (O, *x*, *z*) plane, where *z* is the propagation direction of the incident wave and *x* the direction of the incident electric field. Note that the SH multipolar emission can be easily analyzed by looking at specific directions only, since the electromagnetic fields associated with the different multipoles interfere destructively or constructively when the scattering angle varies [33]. The corresponding 2D emission polar plots are shown in Fig. 2. As observed in the case of the 3D emission patterns, the 2D polar plots clearly reveal the evolution of the nonlinear response with the incident wavelength. For the shortest wavelength, a two-lobe pattern pointing toward the –*z* direction is observed, corresponding to

Optics EXPRESS

SH emission in the backward direction. For the longest wavelength, the same pattern is observed but pointing toward the + z forward direction. On the contrary, a four-lobe pattern is observed for incident wavelengths close to the resonance wavelength. This evolution is easily explained by considering the linear phase as well as the two SH emission channels discussed previously, see Figs. 3(c) and 3(d). Indeed, the SHG from the gold nanorod can be decomposed into a dipolar and a quadrupolar emissions, the relative phase of which depends on both the observation direction and the linear plasmonic phase. However, the latter quantity does not modify the two emission channels in the same manner. Naturally, the quadrupolar emission arises from $E_1 + E_1 \rightarrow E_2$ while the dipolar emission arises from $E_1 + E_2 \rightarrow E_1$, and the fundamental dipolar mode is involved one or two times at the fundamental step. As a consequence, the dipolar and quadrupolar modes are in-phase (out-of-phase) for an incident wavelength longer (shorter) than the resonant wavelength in the + z half-plane. The opposite behavior is observed in the –z half-plane, see Figs. 3(c) and 3(d). Interestingly, in the intermediate case (incident wavelength close to the resonant wavelength), the SH intensity tends to be the same in both half-planes and a pattern with four lobes is observed, Fig. 2(c). Note that a symmetric pattern with four lobes of the same intensity is also possible at specific incident wavelengths. These results clearly demonstrate the role of the phase in a single (uncoupled) nanoparticle. In the following, we show that some of the observed features are also present in complex Fano resonant nanostructures, namely gold nanodolmens.

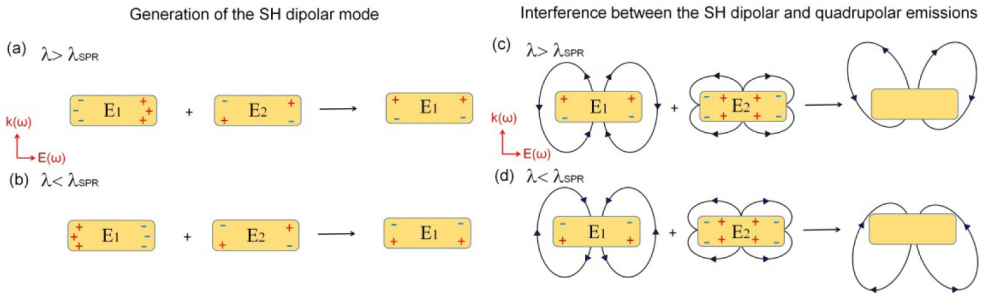

Fig. 3. Influence of the linear phase on the SH emission pattern. (a), (b) Schematics describing the generation of the SH dipolar mode resulting from the $E_1 + E_2 \rightarrow E_1$ mechanism (see the text for details). (c) For an excitation wavelength λ longer than the surface plasmon resonance λ_{SPR}, the SH dipolar and quadrupolar emissions are in phase in the forward direction. (d) For an excitation wavelength λ shorter than the surface plasmon resonance λ_{SPR}, the SH dipolar and quadrupolar emission are in phase in the backward direction.

3.2 Gold nanodolmen

The plasmonic dolmen studied here is composed of three gold nanorods [15–17], identical to the one studied in the previous section (dimensions: 120 nm x 40 nm x 40 nm). Two nanorods are parallel to each other and the third nanorod is perpendicular to them, Fig. 4. The incident planewave is polarized along the latter nanorod (x-axis). The dipolar moments of the horizontal nanorod and of the left vertical nanorod have been computed along the x-axis and along the y-axis, respectively, as a function of the incident wavelength, Figs. 4(a) and 4(c). Contrary to the case of a single nanorod, the amplitudes of the dipolar moments do not correspond to a Lorentzian function but reveal asymmetric lineshapes characterized by two maxima. These lineshapes, which are different, are typical features of Fano resonances [10, 11]. In the present case, the Fano resonance arises from the interference between a dipolar bright mode, supported by the nanorod aligned along the x-direction, and a dark quadrupolar mode, supported by the two parallel nanorods [15–17]. This quadrupolar mode corresponds to two out-of-phase dipoles supported by each of the parallel nanorods. Due to this interference between the two modes, the evolution of the phase of the dipolar moments with the incident wavelength is not anymore a monotonous function, but a fast variation is clearly observed

Optics EXPRESS

close to the Fano resonance, leading to local maxima and minimum for the dipolar moments around the Fano dip (about λ = 670 nm).

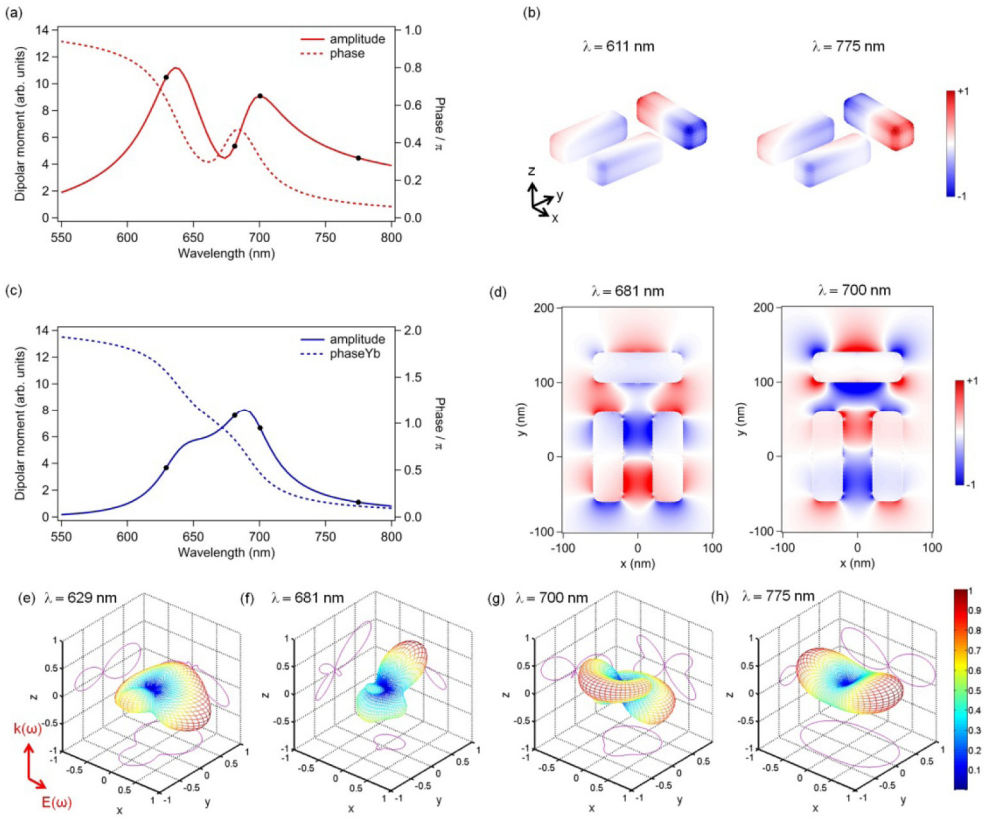

Fig. 4. Linear and SH responses of a plasmonic dolmen composed of three 120 nm x 40 nm x 40 nm gold nanorods. (a) Amplitude and phase of the linear dipolar moment of the top nanorod along the *x*-axis as functions of the incident wavelength. The incident planewave is polarized along the long axis of the top nanorod. The black dots show the wavelength at which the SHG has been studied. (b) Normalized charge distributions for an excitation wavelength shorter (611 nm) and longer (775 nm) than the Fano resonance. (c) Amplitude and phase of the linear dipolar moment of the left vertical nanorod along the *y*-axis as functions of the incident wavelength. The incident planewave is polarized along the long nanorod axis. The black dots show the wavelength at which the SHG has been studied. (d) Real part of the *y*-component of the SH field in the vicinity of the gold dolmen for two incident wavelengths close to the Fano resonance. SH emission patterns for the gold dolmen for four different incident wavelengths: (e) λ = 629 nm, (f) λ = 681 nm, (g) λ = 700 nm, and (h) λ = 775 nm.

Having determined the linear response of the gold dolmen, we turn our attention to its SHG. Figures 4(e)–4(h) show the SH emission patterns computed for four distinct incident wavelengths, covering the spectral range of the Fano resonance. The results reveal that the SH emission pattern dramatically depends on the incident wavelength, even more than in the case of a single nanorod. This observation is attributed to the non-centrosymmetric shape of the gold dolmen, which results in a low number of symmetry planes and less restrictive rules determining the direction of the maximal SH intensity. It is interesting to see that a 20 nm wavelength shift close to the Fano dip is able to completely flip the direction of the maximal SH intensity, compare panels (f) and (g) in Fig. 4, while the same flip requires a larger wavelength shift for a single nanorod, see Figs. 1(c) and 1(e). This effect is also visible in the SH electric field close to the gold dolmen. The comparison between the two panels in Fig. 4(d) clearly reveals that the SH electric field close to the vertical nanorods flips, although this

Optics EXPRESS

is not the case close to the horizontal nanorod. Note that the SH electric field has the same phase close to the two parallel nanorods as reported for split ring resonators [72, 73].

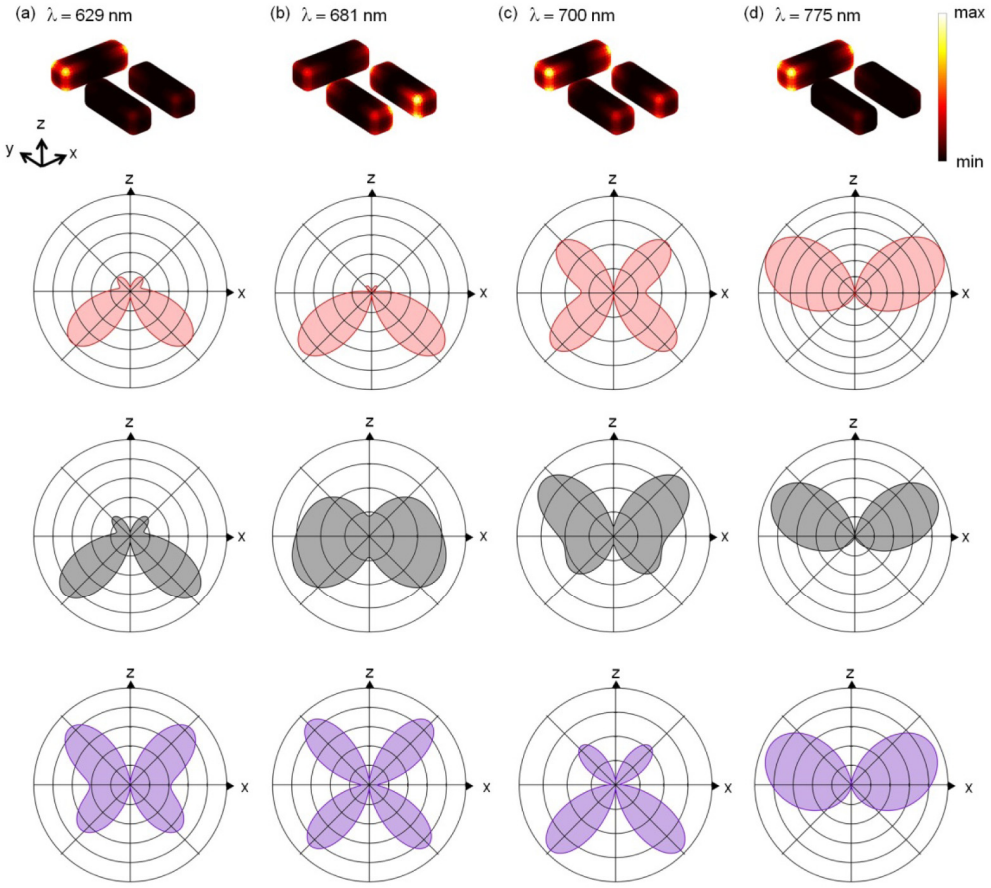

Fig. 5. Nonlinear polarization distribution on the surface of a gold nanodolmen and the corresponding second harmonic generation emission patterns in the (O, x, z) plane for four different incident wavelengths: (a) λ = 629 nm, (b) λ = 681 nm, (c) λ = 700 nm, and (d) λ = 775 nm. The total second harmonic signal, the second harmonic signal from the top nanorod, and the second harmonic signal from the two parallel nanorods are shown in red (top line), black (intermediate line), and purple (bottom line), respectively.

In order to understand this dramatic evolution of the nonlinear response, we have decomposed the total SH emission into the contributions of its constituting elements, the two parallel nanorods and the horizontal one, following a numerical procedure previously developed for the investigation of the nonlinear mode coupling in the SHG from double resonant nanoantennas [74]. In this approach, the SH sources standing at the surface of the considered nanoparticle are conserved and the ones standing at the surface of the other nanoparticles are removed. The SH emission patterns in the (O, *x*, *z*) plane are shown in Fig. 5 for an incident wavelength ranging from λ = 629 nm to 775 nm. For the longest wavelength (λ = 775 nm), the complete gold dolmen, the nanorod along the *x*-direction, and the two parallel nanorods have the same SH emission patterns, Fig. 5(d). The SHG from the two parallel nanorods is low in this specific case since the coupling between the bright and the dark modes is weak at this wavelength, as revealed by the nonlinear surface polarization, top panel in Fig. 5(d). The observed emission pattern also corresponds to the one observed for a single nanorod for the same incident wavelength, see Fig. 2(e), emphasizing that the phase

Optics EXPRESS

results in identical features in distinct plasmonic systems, at least in the weak coupling regime. The same observation is made at the shortest wavelength (λ = 629 nm). This is not surprising because, for this wavelength, the mode coupling at the fundamental wavelength is also weak. For intermediate wavelengths, the SH sources are distributed over the entire gold dolmen, see Figs. 5(b) and 5(c). As a consequence, the total SH emission and the contribution from the top nanorod are not identical in this spectral range, and the total emission patterns cannot be assigned to a reduced number of nanorods in this case. However, the interference between the nonlinear emissions from the different nanorods is responsible for the substantial tuning of the nonlinear response for incident wavelength close to the Fano dip. Indeed, the interference between the emission from the different SH sources is a physical process very sensitive to the evolution of their relative phase.

4. Conclusions

In summary, we have numerically studied the SHG from a single gold nanorod and from a Fano resonant metamolecules composed of three nanorods arranged in a dolmen structure. The results emphasize the important role played by the linear phase in the nonlinear response of the system. Indeed, the interference between the SH modes supported by the system depends on their relative phase, which is deeply related to the phase of the linear modes. This has important implications for experiments, because the SHG can be suppressed in the direction in which the nonlinear signal is recorded, despite an overall strong SHG. Furthermore, the complex phase evolution associated with a Fano resonance arising at the fundamental wavelength enables controlling the SH emission patterns from plasmonic metamolecules over a narrow spectral range with a very good precision. This will be useful for the design of nonlinear plasmonic metasurfaces with new functionalities [75–77]. For example, this property can be exploited in the fabrication of nonlinear plasmonic color routers pumped with ultrashort, spectrally broad, femtosecond pulses resulting in the scattering of the different spectral components of the SH wave in distinct but well-controlled directions [78], extending plasmonic color routers to the nonlinear regime [79, 80].

Funding

Swiss National Science Foundation, SNSF (Project 200020_153662).